Building and Environment 186 (2020) 107348

Contents lists available at ScienceDirect

Building and Environment

journal homepage: http://www.elsevier.com/locate/buildenv

Numerical simulation of air pollution mitigation by means of photocatalytic coatings in real-world street canyons

Beatrice Pulvirenti [a,*], Sara Baldazzi [a], Francesco Barbano [b], Erika Brattich [b], Silvana Di Sabatino [b]

[a] Department of Industrial Engineering, Alma Mater Studiorum, University of Bologna, viale del Risorgimento 2, 40136, Bologna, Italy
[b] Department of Physics and Astronomy DIFA, Alma Mater Studiorum, University of Bologna, via Irnerio 46, 40127, Bologna, Italy

ARTICLE INFO

Keywords:
Photocatalytic-coating
Street canyons
Pollutant removal
Field data
CFD simulations

ABSTRACT

Motivated by the increasing interest on passive control solutions to lower pollutant concentrations in cities, this paper introduces a novel methodology to demonstrate the potential of photocatalytic coatings in abating air pollution in real-world urban environments. The methodology introduced in this paper is based on an original application of Computational Fluid Dynamic (CFD) modelling to simulate the effect of photocatalytic coatings in real yet simplified urban setting. The numerical approach is validated against observations gathered during an ad-hoc designed intensive experimental campaign performed in a real urban area in the city of Bologna, Italy (44.5075 N, 11.3514E), under semi-controlled conditions. Comparison of the model output with observations show a concentration reduction in the range 10–20%. After validation and choice of the proper model set-up, numerical simulations are analyzed by focusing on the mechanisms enhancing the flow circulation within the canyon, an effect that may increase the effect of coatings within street canyons. Results show that application of photocatalytic coatings can give pollutant reductions up to 50% in a confined region close to the walls. A parametrization for the pollutant reduction within the street canyon is suggested to summarize these results, providing a characterization of the photocatalytic coatings performances as a function of the geometric characteristic of the street canyon.

1. Introduction

The ever-increasing urbanization of modern cities and related environmental problems is pushing society to find novel solutions to mitigate air pollution. In this framework, passive control systems (PCS) are being explored as a possible mean to mitigate urban air pollution. Among the PCS used at street level to lower air pollutant concentrations, photocatalysis has been introduced quite recently with the aim to transform harmful substances for human health into inert salts not directly affecting human respiration. In particular, titanium oxide compounds (TiO_2), activated by UV solar radiation, react with the nitrogen oxides (NO_x), sulfur oxides (SO_x) and organic substances (OC) present in air, also in the form of atmospheric particulate matter (PM), producing inert particles that adhere to the wall to which the coatings have been applied. This technique is based on a physical mechanism similar to photosynthesis: the UV radiation acts on the coating layer, generating electron-hole pairs, which in turn generate very reactive free radicals (OH), which combine with the pollutants transforming them into inert particles such as nitrates sodium ($NaNO_3$) or calcium nitrate ($Ca_2(NO_3)_2$). Although the use of photocatalytic coatings (PC) in the real atmosphere is still in the experimental phase and the scientific literature on the subject has not yet reached a consensus, these paints have been extensively tested in laboratories, showing that they can produce an absorption up to 50% of the nitrogen oxides they are in contact with [1], and they can degrade nanometric organic particles such as virus [2].

Few experiments are reported in the literature on the effectiveness of photocatalytic coatings conducted outdoors, in an urban environment [3-5]. These works demonstrate on the one hand that it is possible to experimentally evaluate the capacity of some of these photocatalytic coatings to remove pollution and to quantify the amount of the pollution removed. On the other hand, these analyses are weak in absence of numerical models able to simulate the phenomenon, since all mechanisms that affect the urban environment are strongly influenced by local atmospheric conditions and therefore subjected to large variability.

* Corresponding author.
E-mail address: beatrice.pulvirenti@unibo.it (B. Pulvirenti).

https://doi.org/10.1016/j.buildenv.2020.107348
Received 14 April 2020; Received in revised form 8 September 2020; Accepted 28 September 2020
Available online 1 October 2020

[6] reported on an experiment conducted inside the Umberto I tunnel, in the center of Rome, Italy to evaluate the application of interior coating, in locations with little availability of ultra violet (UV) radiation. The location was chosen by virtue of the relative low variety of elements affecting the results. The main parameters considered were the airflow and the vehicles passing through the tunnel. The measurements, compared with the reference data measured by standard air quality stations showed a reduction of NO_x exceeding 20%, with peaks of over 50% during the summer period, when the availability of UV rays at the entrance to the tunnel increases. Gallus et al. [7] reported the results of an experimental field campaign conducted in the Leopold II tunnel in Brussels (Belgium) to verify the effects of photocatalytic cementitious coating materials applied on the side walls and ceiling. In this case, the comparison of NO_x pollutant concentrations measured before and after the application of the photocatalytic coating indicated a reduction lower than the 2%. Further laboratory analyses indicated that the photocatalytic material showed a serious deactivation under the heavily polluted tunnel conditions and that the UVA irradiance provided by UV lamps to activate the photocatalysis in the tunnel was below the targeted values. Full-scale experiments performed on a real urban street canyon (Castorweg street in Hengelo, The Netherlands) were reported by Ballari et al. [8]. Concrete pavement blocks were added with TiO_2 based photocatalytic material and substituted in half of the street while the other half was covered by untreated blocks. NO_x concentrations measured in one half of the street covered with concrete blocks added with TiO_2 based photocatalytic material were compared with those measured in the other half covered with untreated blocks and used as control site. The comparison indicated that the NO_x reduction by the photocatalytic coatings depended on the weather conditions, with peaks of 28% soon after the application of the photocatalytic material. Maggos et al. [9] measured the photocatalytic properties of a construction material under real meteorological conditions with a controlled pollution release within street canyons build *ad hoc* in order to allow a real scale laboratory test. NO_x concentrations were measured contemporarily during summer in three parallel artificial street canyons, of which one treated with photocatalytic material; the results indicated reductions in the range 37–82% very close to the canyon walls (15–30 cm), depending on the wind direction.

Very few works have previously attempted to simulate the effects of the photocatalytic coatings at a neighborhood scale, meaning considering the influence of surrounding geometry with respect to the focus area. Jeanjean et al. [10,11] compared the effect of different pollutant mitigation measures, including photocatalytic coatings, by means of CFD (Computational Fluid Dynamic) approaches. In particular, the NO_x removal action exerted by the photocatalytic coatings was simulated by means of a deposition model similar to that used to model the pollutant deposition on plants. However, this effect has not been validated in their paper probably due to a lack of comprehensive data sets. In an attempt to compare different pollutant mitigation measures, the model approach discussed in Jeanjean et al. [10,11] was applied to different scenarios in a real street in London (Oxford street), showing that the addition of photocatalytic coatings to building surfaces present minimal improvement to the overall air quality. Nevertheless, their results also indicated that photocatalytic coatings can significantly lower NO_x concentrations in street canyons near the hotspots, depending on the street geometry and orientation with respect to the wind direction. None of the works currently available in the literature, at our knowledge, provide a reliable and validated CFD model that can be applied to complex urban features in presence of photocatalytic coatings.

In this paper, we present a novel CFD-based approach to model the effect of photocatalytic coatings on the local distribution of NO concentration within real street canyons. The numerical model has been validated with observations gathered within an ad-hoc designed intensive experimental field campaign performed in real street canyons in an urban area located in the outskirt of the city of Bologna (44.5075 N, 11.3514E), in northern Italy. These experiments were conducted as part of the iSCAPE ("Improving the Smart Control of Air Pollution in Europe") H2020 project during August 2018.

Briefly, two street canyons characterized by the same geographical orientation were identified in the area, and instrumented for measurements of air quality and meteorology, with the aim to assess the effectiveness of the photocatalytic coatings in reducing NO_x concentrations in urban street canyons. To this purpose, several controlled releases were conducted during specific meteorological conditions selected with respect to atmospheric forcing acting on the area to facilitate establishment of local circulations. Measurements conducted within the experimental campaign were used to compare the numerical results and to set a calibration and a verification of the simulation of pollutant reduction by photocatalytic coatings at the wall. The model has been used to analyze the effect of photocatalytic coatings in real urban street canyons and its dependence on meteorological conditions and urban geometry with the scope of finding parameters able to describe the effectiveness of the coatings over different real urban geometries.

After this Introduction, in Section 2 the experimental campaign is described. A description of the numerical models used for the simulations is provided in Section 3 and some results are discussed in Section 4.

2. Site description and measurements

2.1. Site description

The field campaign took place in the outskirt of Bologna, namely the Lazzaretto area. This area comprises a major street (Terracini street) with smaller alleys on the east side located within a University campus, is characterized by a low building packing density. To the North-West of Terracini street there is a cluster of buildings surrounded by public greenery. While the streets inside the campus are characterized by reduced traffic, the streets in the surrounding area are characterized by intense car traffic. Two parallel street canyons were identified within the campus (A and B respectively in Fig. 1) with aspect ratios (building height H over width W) $H/W_A = 1.7$ and $H/W_B = 0.9$. Fig. 1 also shows the orientation of the two street canyons with respect to the North-South direction. These sites were then highly instrumented to conduct an intensive experimental field campaign with the aim to assess the effectiveness of photocatalytic coatings in reducing NO_x concentrations in real conditions. The locations of the measurement stations within the two street canyons are shown by triangles in Fig. 1 (right). The red triangles denote the measurement stations at ground level, while the blue triangles denote the measurement stations at roof level.

2.2. Instrumentation setup and measurements

In order to capture the effect of local meteorology on the possible effect of photocatalytic coating, the strategy has been to equip each canyon with fast response instrumentation for both air pollutant concentration, flow, temperature and humidity fields. In the following, we present briefly the instrumentation setup adopted along the experimental field campaign performed during August 2018 in Lazzaretto area. Two mobile laboratories from the Environmental Protection Agency of Emilia-Romagna (ARPAE) equipped for measurements of air quality were deployed in each canyon. Specifically, the two mobile laboratories were equipped for continuous measurements of nitrogen dioxides (NO_x), carbon monoxide (CO), ozone (O_3) with 1-min time resolution, and daily average particulate matter concentrations (PM_{10} and $PM_{2.5}$). Both street canyons have been also equipped with high frequency instrumentation to measure turbulence and meteorological variables at two different height levels within and above the canyons, *i.e.* on the roof of the vans and on the rooftop on the buildings surrounding the canyons. The installation heights in the two street canyons are different, due to the differences in canyon heights: while mid-level instrumentation was deployed at 4 m agl (above ground level) in both canyons, the rooftop level was located at 8 m agl in canyon A and at 12 m

Fig. 1. Overview of the locations of the two street canyons and surrounding area (left) and a different view of the two street canyons A and B (right). The red triangles denote the measurement stations at ground level, while the blue triangles denote the measurement stations at roof level.

agl in canyon B, respectively. The 3D wind field was sampled at 20 Hz with GILL Windmaster sonic anemometers, while measurements of air temperature, air relative humidity and pressure were gathered at 1 Hz sampling rate respectively by HCS2S3 Rotronic thermohygrometers and Vaisala PTB110 barometers. Additional measurements of solar radiation have been performed at 1-min sampling rate on both rooftop locations with CNR4 radiometers (Kipp & Zonen). A summary of the instrumentation setup is presented in Table 1.

Supporting measurements of meteorological variables were retrieved from the local network of meteorological monitoring stations from the ARPAE Environmental Protection Agency located in the city, and specifically from the synoptic meteorological station located on the roof of the highest building of the city, the Asinelli Tower (44.4942 N, 11.3467E; 96 m agl) and from an urban meteorological station located in a major street in the ring surrounding Bologna city center, Silvani street (44.9824 N, 7.4514E; 30 m agl).

During the experimental campaign a total of 8 (6 daytime and 2 fortnight) controlled pollutant releases experiments with a known pollution source (one 19-year-old EURO-2 diesel car) left idling for a fixed time interval of 20 min were carried out in each of the two street canyons. The specific emission factor for an EURO-2 diesel car was obtained from ISPRA (Istituto Superiore per la Protezione e la Ricerca Ambientale), based on EMEP/EEA (European Monitoring and Evaluation Programme/European Environment Agency) air pollutant emission inventory (EEA, 2016) and corresponded to 0.61 g km^{-1} total NO emission, increased of 50% to take into account the mileage of the specific vehicle used in the experiments. During the experiments, the measurements of meteorological parameters were complemented with the measurements of temperature distributions on building façades and ground surfaces in the two street canyons by means of a high-performance FLIR T620 ThermalCAM with uncooled microbolometer, 640 × 480 pixels resolution and an image acquisition frequency of 50–60 Hz collected by an operator. The observations gathered within the controlled pollutant release experiments were used to setup and validate the CFD simulations described in the following sections.

3. Description of the models

In this paper, all the physical phenomena acting within the street canyon together with the photocatalytic coating absorption have been considered, by means of the CD-adapco STAR-CCM + code. The novel part in the numerical approach herein presented is the model of the photocatalytic coating absorption and its interaction with the other models used. In the following sections it is shown the architecture of the numerical approach and the details of each model used.

3.1. Design of the CFD approach

The complex problem described in this paper brings together different physical phenomena that arises within the street canyon,

Table 1
Instrumentation used for meteorological variables and air pollutants measurements.

Instrument type/ principle	Model Instrument	Sampling resolution	Accuracy	Range
Meteorological and turbulence variables				
Sonic anemometer	GILL Windmaster 3D	20 Hz	Wind speed: ±0.01 m s^{-1} Wind direction: ±0.5° @ 12 m s^{-1}	Wind speed: 0–50 m s^{-1} Wind direction: 0–359° Temperature: -40 °C to +70 °C
Thermo-hygrometer	HC2S3-L Campbell Scientific	1 Hz	Temperature: ±0.1 °C at 23 °C Humidity: ±0.8% at 23 °C	Temperature: -40° to +60 °C Humidity: 0–100% non -condensing
Barometer	Vaisala PTB110	1 Hz	±0.3 hPa at +20 °C	500-1100 hPa
Net radiometer	CNR4 Kipp & Zonen	0.02 Hz	Pyranometer spectral response: 305–2800 nm Pyrgeometer spectral response: 4.5–42 μm	Temperature range: -40 to +80 °C
Air pollutants				
Chemiluminescence analyser	Teledyne API Model T200 Chemiluminescence $NO/NO_2/NO_x$ Analyser	0.02 Hz	0.5% of reading above 50 ppb	Min: 0–50 ppb full scale Max: 0–20,000 ppb full scale
Photometric analyser	Thermo Fisher Scientific Inc., Model 49i UV Photometric O_3 Analyser	0.02 Hz	1 ppb	0 to 0.05–200 ppm
Infrared absorption spectroscopy	Teledyne API T300 CO analyser	0.02 Hz	0.5% of reading above 5 ppm	Min: 0–1 ppm full scale Max: 0–1000 ppm full scale
β-attenuation	FAI Swam 5A Monitor	1.16 E−5 Hz	±0.3 μg m^{-3} (24 h cycle, 2.3 m^3/h operating flow rate)	0–50 mg

which usually are considered separately in the literature: turbulence and pollutant diffusion, buoyancy forces driven by temperature differences and the effect of the plants within or around the street canyon microclimate. In this paper all these phenomena are considered together and a novel model at the walls to simulate the action of photocatalytic absorption is included. A schematic of the modelled processes considered is shown in Fig. 2.

The interaction of the various model components i.e. each for each process, implies to check convergency and gridding issues as well as to identify a strategy to reduce the high demanding computational cost. The description of the models, the choice of the set-up, grid domain and convergency of the solution are addressed in the following sections.

3.2. Turbulence and diffusion models

The well-known realizable two-equation k-ε turbulence model was adopted, because it is widely used and tested for various similar cases showing very good agreement with experimental data (see ad instance [12-14]. Under this assumption the transport equation for the kinetic energy k is

$$\frac{\partial}{\partial t}(\rho k)+\nabla\cdot(\rho k u)=\nabla\cdot\left[\left(\mu+\frac{\mu_t}{\sigma_k}\right)\nabla k\right]+P_k-\rho(\varepsilon-\varepsilon_0)+S_k \quad (1)$$

while the equation for the turbulent dissipation rate ε is

$$\frac{\partial}{\partial t}(\rho\varepsilon)+\nabla\cdot(\rho\varepsilon u)=\nabla\cdot\left[\left(\mu+\frac{\mu_t}{\sigma_\varepsilon}\right)\nabla\varepsilon\right]+\frac{1}{T_e}C_{\varepsilon 1}P_\varepsilon-C_{\varepsilon 2}f_2\rho\left(\frac{\varepsilon}{T_e}-\frac{\varepsilon_0}{T_0}\right)+S_\varepsilon \quad (2)$$

where u is the average velocity, μ is the dynamic viscosity of air, σ_k, σ_ε, $C_{\varepsilon 1}$, and $C_{\varepsilon 2}$ are model coefficients. P_k and P_ε are production terms, whose formulation depend on the k-ε model variant, f_2 is a damping function that mimics the decrease of turbulent mixing near the walls, enforcing realizability. S_k and S_ε are used specific source terms, ε_0 is the ambient turbulent dissipation rate value in the source terms, T_e is the large-eddy time scale, T_0 the specific time-scale related to ambient turbulent source term. Mean flow, turbulence, energy and dispersion equations were discretized using a second order schemes and the Semi-Implicit Method for Pressure Linked Equation (SIMPLE) scheme has been used for pressure-velocity coupling. The buoyancy forces have been considered under the Oberbeck-Boussinesq approximation, *i.e.* the mass density is constant in all the terms of the Navier-Stokes equations with exception of the gravitational body force term. The local momentum balance equation then gives:

$$\rho\left(\frac{\partial u_i}{\partial t}+u_j\frac{\partial u_i}{\partial x_j}\right)=\rho g_i-\frac{\partial p}{\partial x_i}+\frac{\partial \tau_{ij}}{\partial x_j} \quad (3)$$

where, the density ρ is assumed to be a function of temperature and pressure in accordance with the ideal gas law:

$$\rho(T,p)=\frac{p}{RT} \quad (4)$$

where R is the specific gas constant, $R=\frac{R_0}{M}$, with $R_0=8314.4621$ (J kmol K^{-1}) and M is the gas molecular weight. For the diffusion model, NO has been used as tracer, where the mass diffusion is computed as:

$$J=-\left(\rho D+\frac{\mu_t}{Sc_t}\right)\nabla Y \quad (5)$$

where D is the molecular diffusion coefficient for the pollutant in the mixture, $\mu_t=\rho\left(\frac{C_\mu k^2}{\varepsilon}\right)$ is the turbulent viscosity, Y is the mass fraction of the pollutant, ρ is the mixture density. In Eq. (5), $Sc_t=\frac{\mu_t}{\rho D_t}=0.7$ is the turbulent Schmidt number, where D_t is the turbulent diffusivity. The pollutant source has been simulated by separating volumes with dimension 0.5 m × 0.5 m x 0.5 m in the middle of the canyon and by setting a proper NO source on that volume. The choice of using NO is justified by the fact that the simulations were run considering the controlled pollutant release experiments conducted with the EURO-2 diesel car on August 17, 2018, when the primary fresh emissions are constituted mainly by NO (89%) while NO_2 measured in the canyon contained both a primary and a secondary background component not easily separable.

3.3. Model of the photocatalytic effect

In this section a novel method to calculate the effect of photocatalytic coating is presented. It is assumed that the overall effect of photocatalysis on the active surfaces can be attributed to a pollutant flux, S_p (kg m^{-2} s^{-1}), calculated as the product of the reaction velocity V_a (m s^{-1}) and pollutant concentration c (kg m^{-3}), accordingly to Palacios et al. [15]:

$$S_p=-V_a\,c \quad (6)$$

In order to determine the reaction velocity, the following approach has been set. First, a simulation with no NO absorption by the coated walls has been run in order to obtain the average distribution of NO concentration near the wall without photocatalytic effect. Then, a layer with a thickness $d=1$ mm, representing the wall coated with photocatalytic paint has been added to each surface painted with the photocatalytic coatings. In this layer, a NO sink has been added, dividing Eq. (6) by the thickness d of the photocatalytic layer. A first guess value of V_a has been set, as declared by the photocatalytic coating producer [16]. Then, the value of V_a has been iteratively modified until the NO concentration obtained numerically at the position of the measurement station has been found in agreement with the value obtained

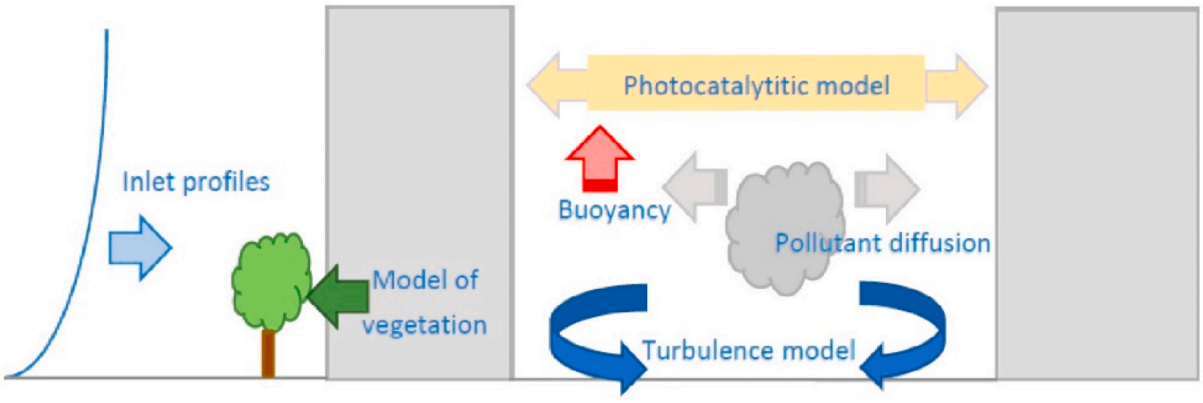

Fig. 2. Schematic of the processes analyzed in the CFD modelling approach. The typical urban inlet profile is also shown.

experimentally. The final value of $V_a = 0.025$ m/s has been obtained. A sensitivity analysis has been made in order to obtain a quantification of the uncertainties related to the method, that has been found under the 10%. That means that the value V_a obtained by this method gives numerical results that differ with experiments less than 10%.

3.4. Model of the effect of vegetation

Some small trees and green walls within the domain considered in this paper has been modelled as sources and sinks of momentum, heat, turbulence kinetic energy and turbulent dissipation rate [17,18]. Similar to other recent works on urban CFD vegetation [10,11], the inertial drag has been parameterized in terms of leaf area density or *LAD* ($m^2\ m^{-3}$) of the vegetation to describe the interactions between foliage and atmosphere, by means of a momentum sink term (Su_j) in momentum equations (one for each velocity component) as:

$$S_{U_j} = -\rho LADC_d U u_j \quad (\text{Pa m}^{-1}) \tag{7}$$

where ρ is the air density (kg m^{-3}), u_j is the j wind velocity component (m s^{-1}), U is the average wind speed (m s^{-1}) and C_d is the sectional drag for vegetation (dimensionless). The sectional drag is a constant related to aerodynamic features of vegetation. In this work we assume $C_d = 0.2$, while the value of *LAD* for ivy has been taken as 1.8 ($m^2\ m^{-3}$), according to the value found in literature for ivy [19]. The vegetation also modifies the mean flow motion into wake turbulence. Then, this process is usually parametrized as source and sink terms of turbulent kinetic energy or TKE (k) and turbulent dissipation rate (ε) as follows:

$$S_k = \rho LADC_d\left(\beta_p U^3 - \beta_d U k\right) \tag{8}$$

$$S_\varepsilon = \rho LADC_d\left(C_{\varepsilon 4}\beta_p \frac{\varepsilon}{k} U^3 - C_{\varepsilon 5}\beta_d U \varepsilon\right) \tag{9}$$

where $0 \leq \beta_p \leq 1$ is the fraction of mean kinetic energy converted into TKE by means of drag, β_d is the dimensionless coefficient for the short-circuiting of the turbulence cascade and $C_{\varepsilon 4}$ and $C_{\varepsilon 5}$ are model constants. Several different values of these parameters can be found in the literature; in this work we have used $\beta_p = 1$, $\beta_d = 4$ and $C_{\varepsilon 4} = C_{\varepsilon 4} = 1.5$, according with Buccolieri et al. [20] and Amorim et al. [21]. The pollutant flux S_d (g m^{-2} s^{-1}) is calculated as the product of the *LAD* by the dry deposition velocity V_d (cm s^{-1}) and the pollutant concentration c (g m^{-3}):

$$S_d = -LADV_d c \tag{10}$$

A deposition velocity of $V_d = 1$ cm s^{-1} has been used in this work, according with Santiago et al. [13]. The transpiration cooling of vegetation has been recently included in thermal CFD simulations to evaluate the impact on temperature (Gromke et al. [22]). This effect is modelled by adding a thermal sink P_c (W m^{-3}) that is a function of *LAD*. The same approach is used in this work. The basic principle is that when air flows through vegetation it gets cooled by transpiration, mainly from the leaf surfaces. As suggested by Moradpour et al. [23] a volumetric cooling power of 250 W m^{-3} per unit of *LAD* has been used in this work.

3.5. Discretization and mesh

Different meshes with the same constructive approach have been created for the two street canyons. The computational domain has a size of 950 m × 725 m x 130 m (L x W x H). The height of the tallest building of the street canyon ($H = 13$ m) has been chosen as reference dimension. Given that the maximum reported height in the domain is a building height (H) of 13 m, the computational domain was built with its boundaries placed more than 15H away from the modelled area. The top of the computational domain was set to 130 m, which corresponds to 10H. The dimensions of outer domain give an appropriate mesh size for the required flow detail and run time [12]. The computational domain has been built using unstructured elements with a finer resolution close to the ground and the walls within the neighborhood scale. Several tests have been performed to verify grid size independence with increasing mesh numbers. We achieved grid convergency with a grid with 12.878 million of elements. The convergence criteria have been set to 10^{-8} for the residuals of all the variables considered. The smallest dimension of the elements, in the region near the heated walls, is 0.18 m in the direction normal to the wall. The pollutant sources are modelled as volumes on the ground of the streets. The dimensions of the source section are 0.5 m × 0.5 m x 0.5 m, with the smaller cells having dimensions of 0.05 m. Symmetry boundary conditions have been assigned to the lateral sides and the domain top, a velocity inlet condition was set to the inlet boundary and a pressure outlet condition to the outflow boundary. A no-slip boundary condition was applied at the ground and at the building surfaces.

3.6. Boundary conditions

The boundary and initial conditions set in the simulations derive from the observations gathered during the field campaign previously described in Section 2. Specifically, meteorological observations were obtained from the previously described ARPAE meteorological station located on the Asinelli tower, a 98 m high tower located in the center of the town. At the inflow boundary, vertical profiles for mean velocity u, turbulence kinetic energy k and turbulence dissipation rate ε of the neutrally stratified atmospheric boundary layer were imposed according to Di Sabatino et al. [12,24]:

$$u(z) = \frac{u_*}{k} ln\left(\frac{z + z_0}{z_0}\right) \tag{11}$$

$$k(z) = \frac{u_*^2}{\sqrt{C_\mu}}\left(1 - \frac{z}{\delta}\right) \tag{12}$$

$$\varepsilon(z) = \frac{u_*^3}{kz}\left(1 - \frac{z}{\delta}\right) \tag{13}$$

with z the vertical position above the ground, z_0 the roughness length representative for the terrain windward the computational domain, u_* the friction velocity, $\kappa = 0.42$ the von Karman constant, $C_\mu = 0.09$ and δ the height of the computational domain. The inflow wind profile has been calculated solving Eqs. (11)–(13), using data from the meteorological station, in order to obtain the friction velocity for every different wind condition (Table 2). We set a roughness equal to 0.1 m, according with the literature [12,24].

Uniform temperature profiles have been set, according to the experimental measurements. Observed air pollutant concentrations and meteorological variables recorded inside and above the canyons were used to set and validate the numerical model.

For each direction of the wind, a computational grid has been created in order to have the inlet section perpendicular to the wind.

Temperature boundary conditions have been set at the walls of the street canyons and at the street between the buildings using the

Table 2
Wind direction, wind velocity, friction velocity (u_*) and roughness length representative of the terrain windward the computational domain (z_0) data used to set the boundary conditions.

Case number	Day	Time (UTC)	Wind direction (°) – wind velocity (m s^{-1})	u_* (m s^{-1})	z_0 (m)
1	August 17, 2018	4:00	218° – 3.4	0.21	0.1
2	August 17, 2018	11:00	8° – 2.8	0.21	0.1
3	August 17, 2018	14:00	31° – 2.2	0.16	0.1

previously described measurements with instrumentation deployed at the two height levels in the canyons and from images collected with a thermal camera (Table 3). The temperature of the buildings' façades was obtained from data collected with the IR camera (see section 2.2) during the days of the controlled pollutant releases. In addition, the IR camera was also used to measure the ground temperature and the values obtained from the thermographic images were set into the simulations. The air temperature was obtained by averaging the measurements deployed at two levels (see section 2.2). The results are shown in Table 3.

3.7. Validation tests

The simulations have been validated by comparing hourly values as obtained from the numerical simulations with the measurements performed during the experimental campaign described in the previous section. The NO concentration within the street canyon depends by concentration gradients and by the fluid dynamics i.e. by the meteorological conditions that change in time. We used the experimental values averaged during the release for the comparison with the results of the simulations, checking that the meteorological conditions and the background did not vary during that time interval. The three experiments considered are reported in Table 2 and Table 3 and concern two daylight cases when solar radiation activates the photocatalysis and one fortnight case when no activation of the photocatalytic coating is present. The pollutant source has been simulated by separating a volume with dimensions 0.5 m × 0.5 m x 0.5 m at the ground, in the middle of the canyons, with a NO source of 1.388×10^{-5} kg/m^3 s. The walls and the street in canyon A have been treated with PURETI photocatalytic (see Hassan et al. link). Then, for the simulation of the case August 17, 2018, 11 UTC, the photocatalytic effect has been activated on all the walls and the street, while for the case August 17, 2018, 14 UTC the photocatalytic effect has been activated only on the north walls (see Fig. 1). In order to determine the deposition velocity and the photocatalytic coating model for the PURETI photocatalytic coatings application for the application shown in this paper, the approach described in Section 3.2 has been used. The results obtained by the simulations have been verified through a comparison with the measurements. The results are provided in Table 4.

Table 4 shows good agreement between measured values and simulations for case 1, for canyons A and B. Case 1 has been used to validate the numerical model, while case 2 has been used to set the photocatalytic model. A good agreement has been obtained between measured and simulated NO concentrations in canyon A for case 3. This result provides a validation of the approach herein presented.

4. Results

Local scales atmospheric processes represent the main forcing of ventilation mechanisms in complex terrain (Barlow et al., [25]; Bentham and Britter, [26]; [27]. Thermal and inertial circulations dominate air flows inside a canopy when synoptic conditions are weak [28], commonly referred as geostrophic wind velocity $U_g < 5$ m s^{-1}. Under these conditions, local scales gradients are the key drivers of air flows and the morphology of the terrain plays a fundamental role modifying these gradients or channeling the flow itself [29, 25]. The choice to analyze only small periods within the whole campaign must be considered in view of the most suitable synoptic conditions to study local scale phenomena. Therefore, only few consecutive non-synoptic days (geostrophic wind velocity $U_g < 5$ m/s, clear sky, a wind direction daily pattern typical of the thermal circulation) have been selected for each experimental campaign. This strategy allows us to remove extra forcing affecting the results. As mentioned, the experiments shown in this work were among the first being conducted in real setting. Therefore, in the analysis we select the simpler conditions for reproducing the processes occurring affecting final concentration with and without coated surfaces. Four cases are shown in the following sections. In the first case, no photocatalytic action has been considered on the walls of both the canyons. In case 2, a photocatalytic action on both the walls and the street within canyon A has been considered. In case 3, the photocatalytic effect has been added only on the north wall. Finally, in case 4, the photocatalytic effect has been considered on both the walls and the street within canyon B. The first three cases correspond to real experiments, while the fourth case is virtual.

4.1. Field experiment without the photocatalytic effect

On August 17, 2018 at 4 UTC, the first release experiment (case 1) was performed at night, with the walls of canyon A painted but with the photocatalytic effect not active because of the absence of radiation. The boundary conditions for this case are shown in Tables 2 and 3. The wind direction was from the south-west direction (i.e. the angle between the direction of the wind and the north-south direction was 218°), as shown in Fig. 3. The domain mesh surrounding the buildings was rotated so that the inlet surface was perpendicular to the wind direction, i.e. the axes of the canyons formed a 215° angle with the north-south direction. Fig. 4 (a) shows the streamlines obtained for this case, colored with the wind velocity magnitude, and the NO plumes within the canyons (Fig. 4 (b)). The two canyons in Fig. 4 (a) are highlighted with red rectangles. The north direction has been shown in Fig. 1. The orientation of all the figures where a top view is shown is the same of the one shown in Fig. 1, i.e. north is on the top of the figures where a top view is shown.

Fig. 4 (a) shows that, in canyon A, a spiral-shaped vortex is formed, directed along the axis of the canyon towards the north-west exit of the canyon. This vortex is caused by the air impacting on a wall out of the canyon (right in the figure) that deviates and enters the canyon, creating a forcing that deforms the vortex. In canyon B, a single vortex is formed, presenting the typical shape observed in street canyons with an aspect ratio close to one when the wind direction is perpendicular to the axis of the canyon. This difference in the two vortices creates different shapes of the plumes in the two canyons A and B, as shown Fig. 4 (b). Besides the different shapes, the plumes in the two canyons also present different pollution levels. Fig. 4 presents a focus on the streamlines (Fig. 4 (c)) and the NO plume in canyon A (Fig. 4 (d)) as seen from the east opening of the canyon. The streamlines (Fig. 4 (c)) show that the vortex develops from the bottom towards the top of the canyon, pushing the NO plume to the left wall, as shown by (Fig. 4 (d)). On the west side of the canyon A, the lower part of the canyon is blocked by a layer of climbing ivy that forms a permeable obstacle to the flow. This has been considered in the model, by adding to the geometry a porous wall, with the same numerical approach as that adopted for green infrastructure (GI), as

Table 3
Temperature data used to set the boundary conditions during the experimental campaign.

Case number	Day	Time (UTC)	T_{air} (°C)	Canyon A South façade (°C)	Canyon A North façade (°C)	Canyon A Street (°C)	Canyon B South façade (°C)	Canyon B North façade (°C)	Canyon B Street (°C)
1	August 17, 2018	4:00	21.0	32.0	31.8	30.1	26.0	29.4	26.9
2	August 17, 2018	11:00	30.4	27.3	28.6	43.7	28.3	30.7	44.4
3	August 17, 2018	14:00	31.1	46.0	36.9	36.3	49.5	34.9	32.5

Table 4
Comparison between NO concentrations obtained from the experiments and from the simulations.

Case number	Date	Time (UTC)	Canyon A			Canyon B		
			Measured NO (μg m^{-3})	Simulated NO (μg m^{-3})	Error %	Measured NO (μg /m^{-3})	Simulated NO (μg m^{-3})	Error %
1	August 17, 2018	4:00	103.3	94.9	8.1	119.3	104.8	12.1
2	August 17, 2018	11:00	260.6	269.5	3.4	4.08	6.1	49.5
3	August 17, 2018	14:00	59.8	58.9	1.5	5.28	4.6	20.7

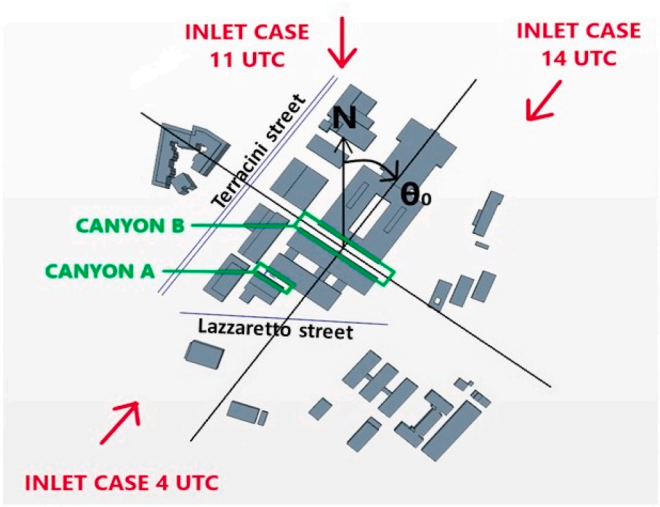

Fig. 3. Orientation of the computational domain for case 1 (August 17, 2018, at 4 UTC), case 2 (August 17, 2018, 11 UTC) and case 3 (August 17, 2018, 14 UTC).

described in Section 3.4. The presence of this GI creates a stagnation in the zone between the source and the west exit of canyon A. Finally, Fig. 4 (e) shows the NO concentration obtained on a vertical plane cutting the measurement station in canyon A and Fig. 4 (f) shows the NO concentration obtained on a vertical plane cutting the measurement station in canyon B. The swirled vortex in canyon A, and the typical vortex that fully occupies canyon B drive the pollutant toward the leeward wall (Fig. 4 (e, f)).

4.2. Field experiment with the photocatalytic effect

The second release (case 2) was performed on August 17, 2018 at 11 UTC, when the painted walls in canyon A and the street were activated by solar radiation. The boundary conditions for this case are shown in Table and Table. The wind direction was from the north direction (*i.e.* the angle between the direction of the wind and the north-south direction was 8°), as shown by Fig. 3. As in the first case, the domain mesh surrounding the buildings was rotated so that the inlet surface was perpendicular with the wind direction. In this case, as shown in Fig. 3, the direction of the wind formed an angle of about 30° with respect to the axes of the canyons. Fig. 5 (a) shows the streamlines, colored with the wind velocity magnitude and the NO plumes within the canyons (Fig. 5 (b)).

In this case, the wind coming from the north creates a wake flow downstream of a group of buildings located just north-east from canyon A (see Fig. 1). The slowed-down flow then propagates into canyon A, where two swirling vortices are formed with very low speed, directed from north-west to south-east. The canyon B is less exposed to this wake flow. The wind enters in canyon B with a swirl with axis parallel to the canyon. Fig. 5 (b) shows that both the plumes are directed towards south-east and pushed toward the north wall. A zoom of streamlines and plume in the canyon A is shown in Fig. 5 (c, d). The dynamics of the flow in this case shows two vortices near the street, occupying only one half of the canyon. The polluted air is pushed toward the top of the canyon by the air on the half of the canyon free by vortices. The presence of these vortices right near the source results in the higher pollutant concentration distribution in proximity of the vortices, as shown in Fig. 5 (canyon A is shown in Fig. 5 (e), while canyon B is shown in Fig. 5(d)). This case has been used as a reference to determine the pollutant sink at the walls, according to Eq. (6). A case with the same boundary conditions, without the photocatalytic effect, has been run in order to obtain the zero activity of the walls. In that case, an increase of NO concentration of 15% at the position of the measurement station has been obtained.

4.3. Field experiment with half photocatalytic effect

The third release experiment (case 3) was performed on August 17, 2018 at 14 UTC, where only the north walls were activated in canyon A by solar radiation. The boundary conditions for this case are shown in Table and Table. The wind direction was from the north-east direction (*i.e.* the angle between the direction of the wind and the north-south direction was 31°), as shown by Fig. 3. As in the previous two cases, the domain mesh surrounding the buildings was rotated in order to have the inlet surface perpendicular to the wind direction. Fig. 6 (a) shows the streamlines obtained for this case, colored with the wind velocity magnitude and the NO plumes obtained within the canyons (Fig. 6 (b)). The wind in this case comes from the opposite direction with respect to case 1. Therefore, the vortices within the canyons in this case show a rotation in the opposite direction with respect to the first case. Two similar vortices are formed within the canyons A and B, that do not cover the entire length of the canyons because are broken by a mixing flow in the middle of the canyon due to the inclination of the canyon with respect to the wind direction. Fig. 6 (b) shows that the plumes are close to the north wall, but for canyon A the plume occupies almost the whole volume between the walls.

A zoom of streamlines and plume in the canyon A is shown in Fig. 6 (c,d). The dynamics of the flow in this case is again more complex. Two vortices are present within the canyon, one near the street, with axis parallel to the canyon and one in the upper part of the canyon, with axis perpendicular to the canyon axis. The upper vortex drives the polluted air toward the top of the canyon, as shown by Fig. 6 (c). The presence of these vortices right near the source gives the pollutant concentration distribution shown in Fig. 6 (e, f) on vertical planes obtained cutting the position of the measurement stations (canyon A is shown in Fig. 6 (e), while canyon B is shown in Fig. 6 (f)). A case with the same boundary conditions without the photocatalytic effect has been run in order to compare these results with the case of no photocatalytic activity at the walls. In that case, an increase of NO concentration of 18% at the position of the measurement station has been obtained. Fig. 7 shows NO concentrations on a vertical plane cutting the position of the NO source on canyon A, along the z vertical direction, at 25 cm and 50 cm distance from the north wall. Fig. 7 shows that, for $z < 5$ m, a reduction of NO concentration is obtained, with values that, in the lower part of the canyon near the wall, reach a reduction of pollutant concentration up to 40%.

The maximum of the NO reduction is obtained at a height of 1 m and the reduction is large for $z < 2$ m, which proves that the effect is important for all human beings with a larger effect for children at $z = 1$ m.

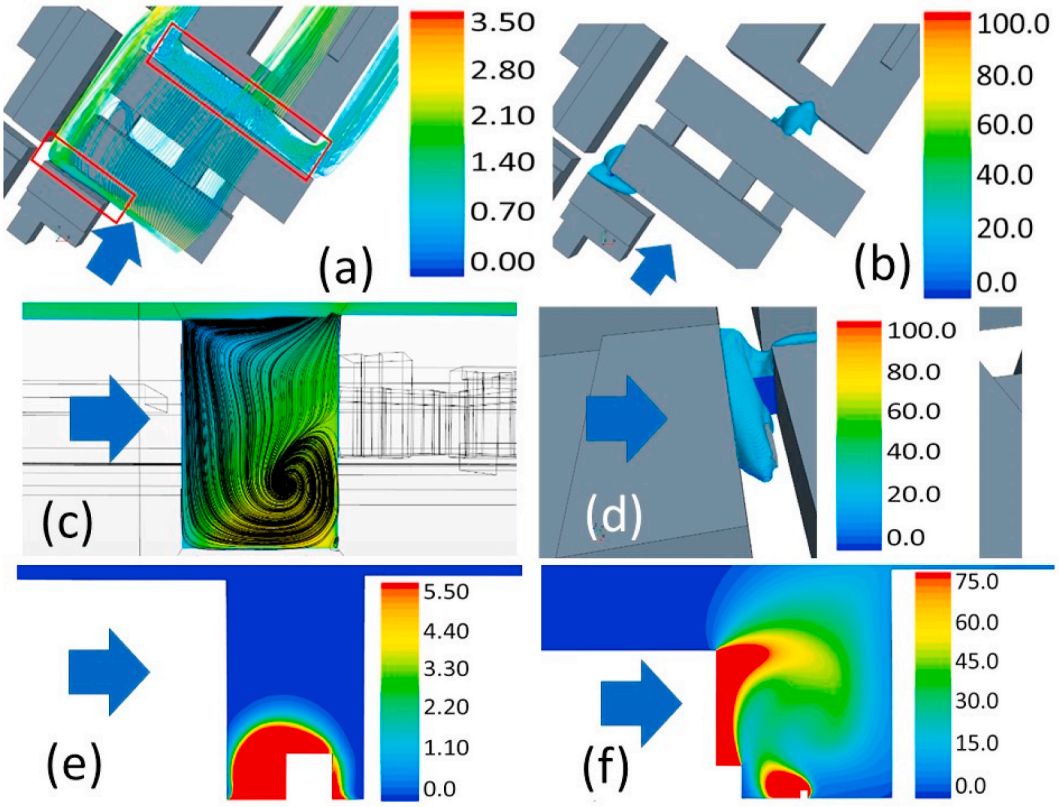

Fig. 4. Case 1, (August 17, 2018, 4 UTC). (a): streamlines colored with wind velocity magnitude (m s^{-1}). (b): NO plume obtained for a value of NO concentration at 20 (μg m^{-3}). (c): streamlines on a vertical surface in the middle of canyon A. (d): zoom of the NO plume in canyon A obtained for a value of NO concentration at 20 (μg m^{-3}). (e): NO concentration (μg m^{-3}) on a vertical planes at the location of the measuring station in canyon A. (f) NO concentration (μg m^{-3}) on a vertical plane at the location of the measuring station in canyon B. Blue arrows show the direction of the wind.

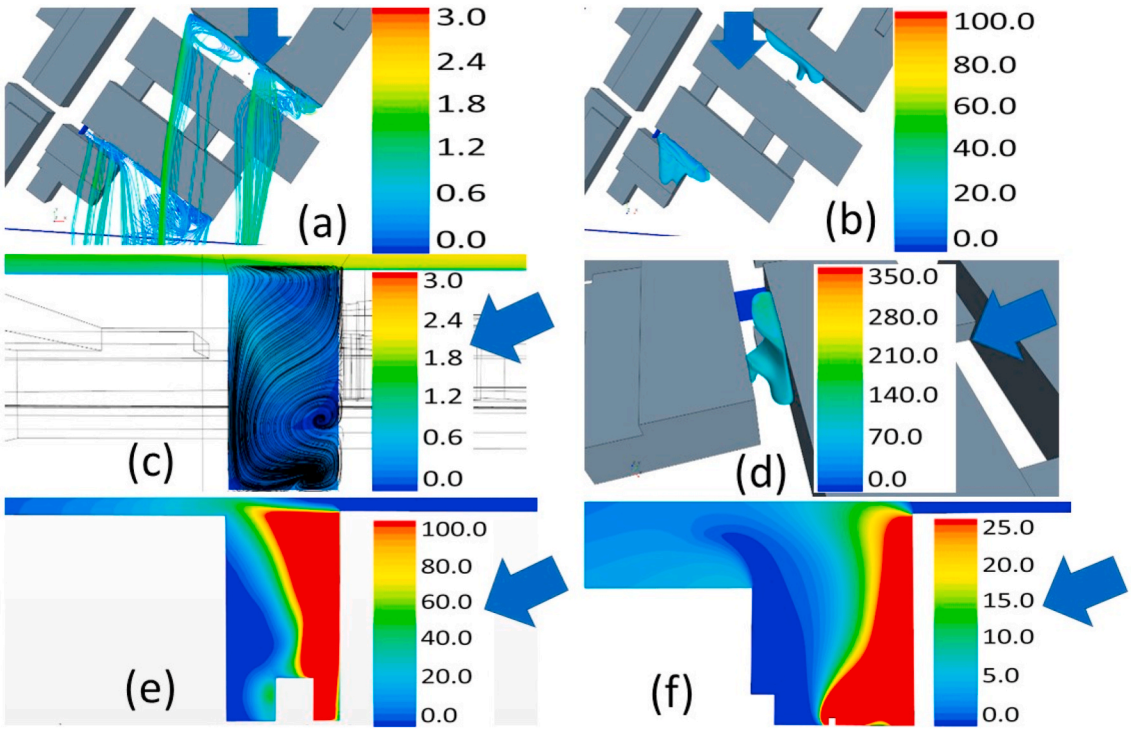

Fig. 5. Case 2, (August 17, 2018, 11 UTC). (a): streamlines colored with wind velocity (m s^{-1}). (b): NO plume shape obtained for a value of NO concentration at 20 (μg m^{-3}). (c): streamlines on a vertical surface in the middle of canyon A. (d): zoom of the shape of the NO plume in canyon A obtained for a value of NO concentration at 80 (μg m^{-3}). (e): NO concentration (μg m^{-3}) on a vertical planes at the location of the measuring station in canyon A. (f) NO concentration (μg m^{-3}) on a vertical plane at the location of the measuring station in canyon B. Blue arrows show the direction of the wind.

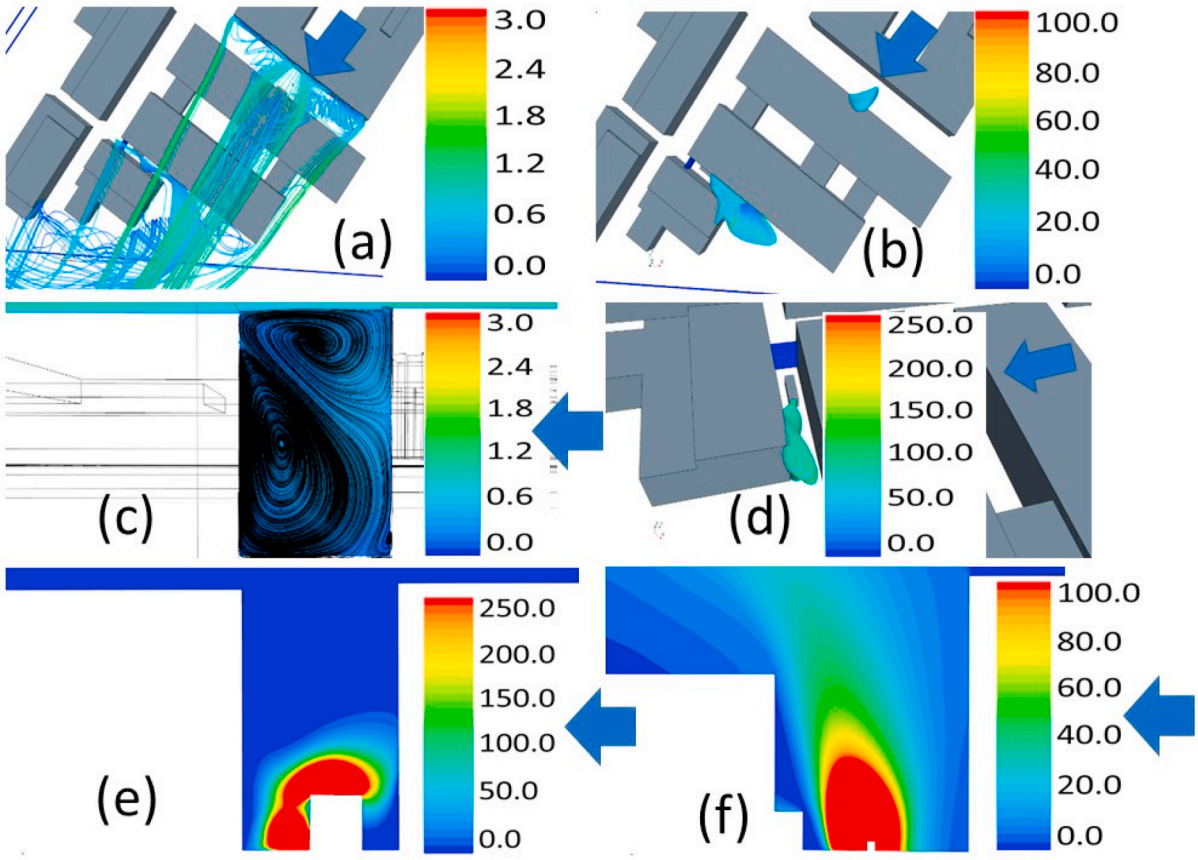

Fig. 6. Case 3, (August 17, 2018, 14 UTC). (a): streamlines colored with wind velocity (m s^{-1}). (b): NO plume shape obtained for a value of NO concentration at 20 (μg m^{-3}). (c): streamlines on a vertical surface in the middle of canyon A. (d): zoom of the shape of the NO plume in canyon A obtained for a value of NO concentration at 80 (μg m^{-3}). (e): NO concentration (μg m^{-3}) on a vertical planes at the location of the measuring station in canyon A. (f) NO concentration (μg m^{-3}) on a vertical plane at the location of the measuring station in canyon B. Blue arrows show the direction of the wind.

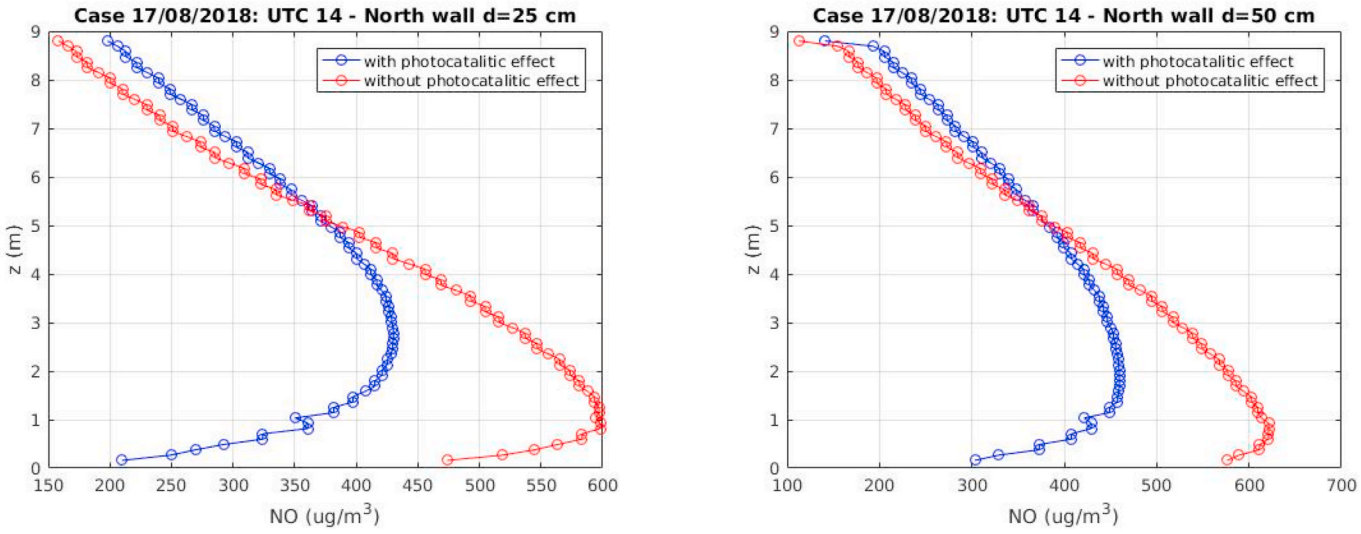

Fig. 7. Canyon A: profiles of NO concentration (μg m^{-3}) obtained for case 3: August 17, 2018, 14 UTC. Left: profiles of NO concentration (μg m^{-3}) at 25 cm from the north wall; right: NO concentration profile at 50 cm from the north wall.

4.4. Virtual release with photocatalytic effect

This case (case 4) corresponds to a virtual release conducted under the same meteorological boundary conditions of case 3 (considered in section 4.3), considering canyon B walls painted with photocatalytic coatings. The difference with the previous cases is that a line source of NO corresponding to 10 EURO-2 diesel cars with the same characteristic as that considered in the previous experiments has been added to the middle of canyon B, *i.e.* a NO source of 1.388×10^{-5} kg/(m^3 s). This case is compared with a case with the same NO production in the middle of

the canyon, but with no activation of photocatalytic coatings on the walls. Fig. 8 (a) shows the streamlines obtained for this case, colored with the wind velocity magnitude and the NO plumes within the canyons (Fig. 8 (b)). Fig. 8 (b) shows that the NO plume in canyon B is close to the north wall, occupying half of the canyon. Fig. 8 (c, d) shows NO concentration distributions obtained on a vertical plane in the middle of the canyon. Fig. 8 (c) shows the same case without the photocatalytic and Fig. 8 (d) shows the case with photocatalytic effect. The comparison between Fig. 8 (c) and Fig. 8 (d) shows that the reduction of NO concentration is relevant only close to the walls.

Fig. 9 shows the streamlines (a) and NO concentration patterns (b, c) obtained on a vertical section of canyon B at a distance of 20 m from the middle of the canyon in the east direction. Fig. 9 (b) shows the case without photocatalytic effect, while Fig. 9 (c) shows the case with the photocatalytic effect. Two vortices with very similar patterns and with about the same dimensions can be observed in Fig. 9 (a). A strong effect of the photocatalytic coating is obtained, due to the position of the vortex close to the leeward wall.

Fig. 10 presents the vertical profiles of simulated NO concentration, at 25 cm and 50 cm distance from the north wall. The figure shows a significant reduction of NO concentration, with values up to 40% near the wall in the lower part of the canyon. The maximum NO reduction is observed for $z < 2$ m, which means that close to the walls the effect of photocatalytic absorption of pollutants is important for all human beings with a larger effect for children.

4.5. Discussion of the results

The analysis of the cases herein presented demonstrates that the complex action of the photocatalysis can be studied by means of a CFD approach. In order to find dimensionless parameters useful to represent the photocatalytic action within the street canyon, the following variables can be introduced.

- Street canyon aspect ratio

where H is the height of the canyon and W is the width.

- Total area painted with photocatalytic coatings divided by the volume of the street canyon

where S_p is the area of walls painted with photocatalytic coatings and V_c is the volume of the street canyon ($V_c = HWL$, where L is the length of the canyon).

- NO reduction

where $\dot{M}_{NO_{abs}}$ is the mass flow rate of NO absorbed by the painted surfaces (μg/s) and $\dot{M}_{NO_{em}}$ is the mass flow rate of NO emitted within the street canyon (μg/s).

- Mass flux of NO absorbed per coated area, $\dot{m}_{NO_{abs}} = \frac{\dot{M}_{NO_{abs}}}{S_p}$ (μg/s m^2).
- Normalized NO reduction within the canyon,

$$NO^* = \frac{NO_{with-ph}}{NO_{without-ph}}$$

i.e. the spatial average of NO concentration obtained within the canyon with the photocatalytic action, divided by the spatial average of NO concentration obtained within the canyon without the photocatalytic action [30]. The spatial average of NO concentration within the canyon is obtained as an integral over the volume of the canyon, i.e. $NO = \frac{1}{V_c}\int_{V_c} NO\, dV$

These parameters are shown in Table 5 for the street canyons considered in sections 4.2, 4.3 and 4.4 (cases 2, 3 and 4 respectively).

Table 5 shows that the NO reduction, NO_{red} is higher than 40% for cases 2 and 3, *i.e.* for the cases with canyon A coated, while, for case 4, NO_{red} is one third of that obtained for case 2. This result shows the dependence of the photocatalytic absorption on the shape of the canyon, *i.e.* the aspect ratio. These result suggest that the aspect ratio could be an important factor to enhance the photocatalytic effect in a street canyon. However, as the aspect ratio increases, the time in which the surfaces are exposed to sunlight decreases. The average of NO concentration over the canyon volume has been introduced, to present a measure of the volumetric action of the photocatalytic coating within the canyon. Then, a normalized NO reduction NO^* has been introduced, where the average over the volume of the street canyon of NO concentration where there is a photocatalytic effect has been divided by the average of NO concentration obtained within the same street canyon with no photocatalytic effect. In the three cases the value of NO* is between 0.79 and 0.84, *i.e.* the photocatalytic effect in the real application shown in this paper gives an average NO reduction within the canyon in the range 14%–20%. The

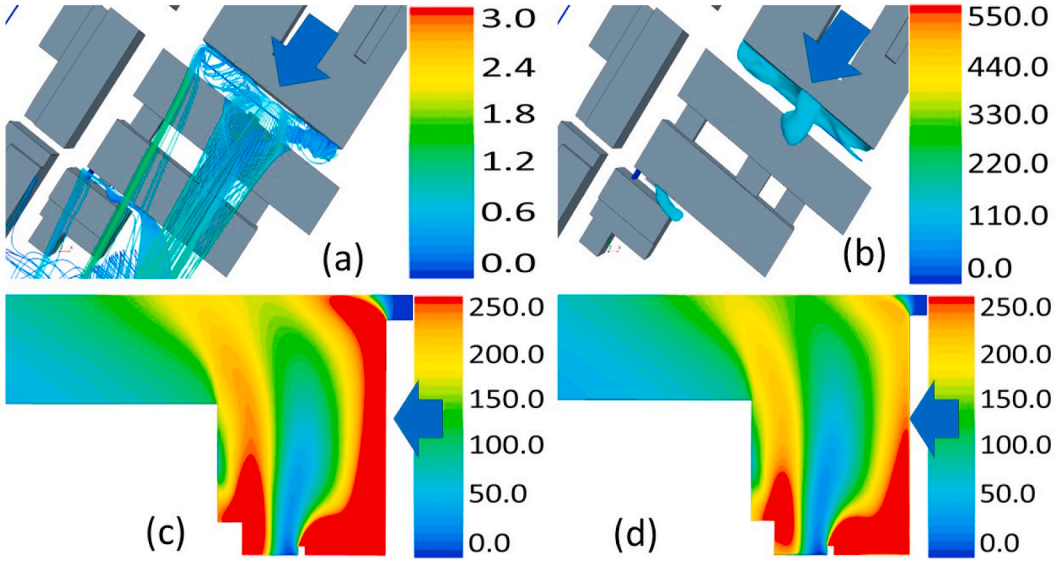

Fig. 8. Case 4. Streamlines colored with wind velocity (m s^{-1}) (a) and NO plume shape obtained for a value of NO concentration at 120 (μg m^{-3}) (b). NO concentration (μg m^{-3}) on a vertical plane in the middle of canyon B (c: without photocatalytic effect; d: with photocatalytic effect). Blue arrows show the direction of the wind.

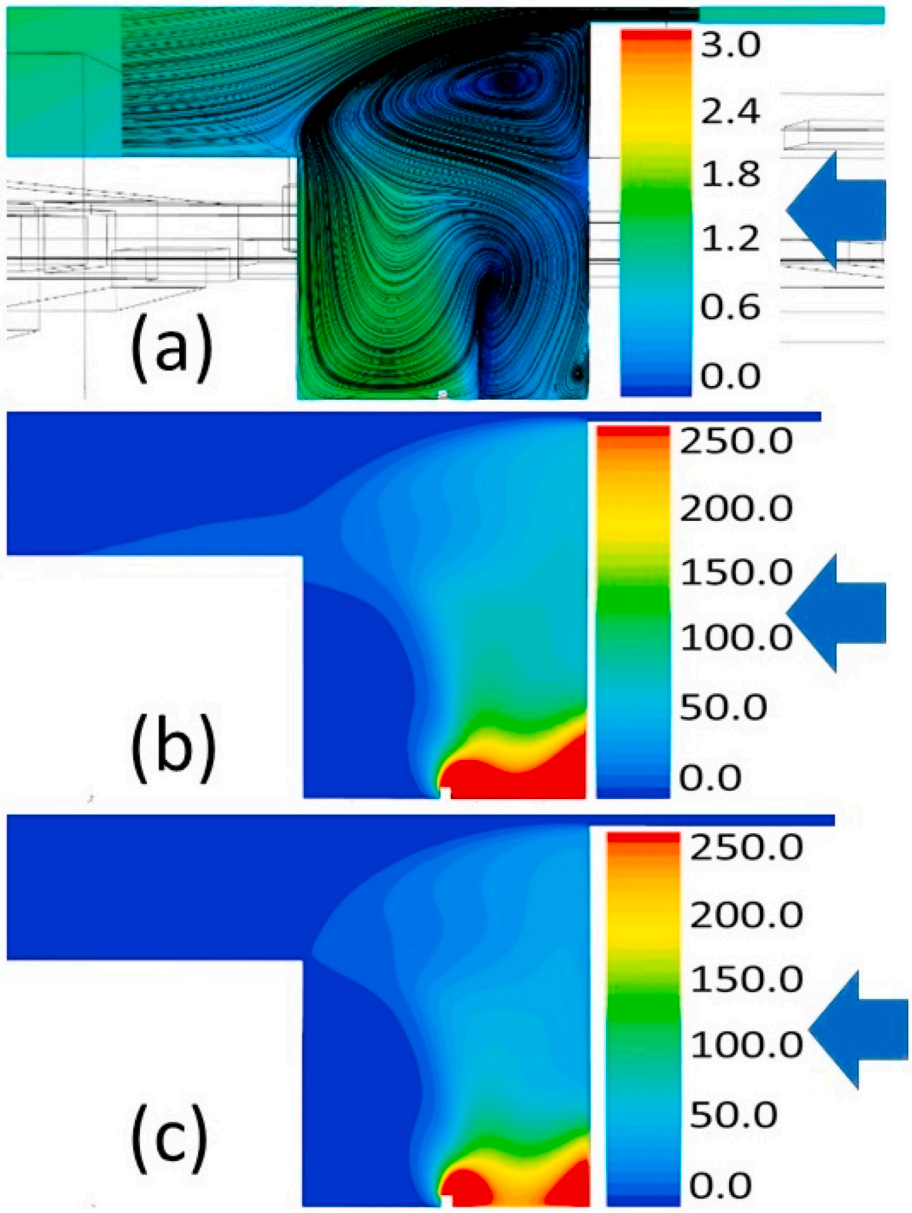

Fig. 9. Case 4. (a) streamlines and velocity magnitude (m/s); (b) NO concentration (μg/m^3) without photocatalytic effect; (b) NO concentration (μg/m^3) with photocatalytic effect. Blue arrows show the direction of the wind.

parameter NO^* is independent from the street canyon geometry and can be used to represent the pollutant reduction by means of photocatalytic coatings within urban geometries in upscaled or integral approaches such as those implied using simpler models than CFD such ADMS-Urban [31].

5. Conclusions

This work presents a novel CFD approach to evaluate the effect of photocatalytic coatings in a real urban street canyon. The idea of this paper is that the pollutant capturing effect is enhanced by the well-known confined flow regimes that usually establish within street canyons. The numerical approach is validated against measurements gathered within an ad-hoc designed intensive experimental campaign performed in a real urban area in the city of Bologna, Italy under semi-controlled conditions. Through the CFD approach, the local distribution of NO concentration within the canyon has been obtained for the same conditions of the experiments. The comparison of the simulated concentrations with observed ones was used to conduct a preliminary calibration of the model of pollutant reduction by the photocatalytic coatings. Following the choice of the proper set-up, the model was applied to analyze the outputs under other meteorological conditions typical of the summer season encountered during the experimental campaign. The analysis of the simulations indicate that the NO reduction is limited in a volume close to the walls and can reach higher values than those determined from a detailed data analysis of the observations collected within the experimental campaign (in the range 10–20%; a result that will be discussed by the authors in a different paper) and up to 40–50% near the coated walls. The analysis of the numerical outputs also suggest that the NO reduction is a function of the atmospheric conditions (wind velocity and wind direction, temperature, solar radiation) together with the geometry of the real street canyons. Moreover, it is necessary to consider that, as the aspect ratio increases, the time in which the surfaces are exposed to sunlight decreases. In order to summarize these results, some indicators of the performances of the photocatalytic coatings have been introduced. For instance, the NO

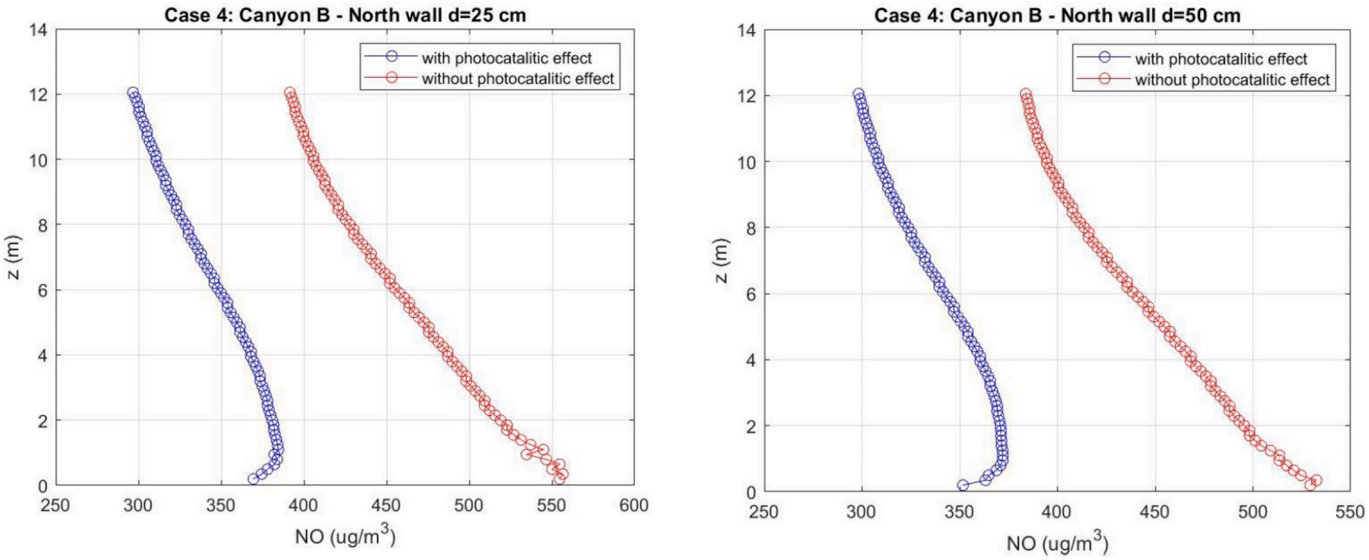

Fig. 10. Canyon A: profiles of NO concentration (μg m^{-3}) obtained for case 4. Left: profiles of NO concentration (μg m^{-3}) at 25 cm from the north wall; right: NO concentration profile at 50 cm from the north wall.

Table 5
Characteristic parameters for the street canyon painted with photocatalytic coatings.

Case	Canyon aspect ratio $\alpha = H/W$	Coated area per canyon volume $\rho = S/V_c$ (m^{-1})	NO reduction $NO_{red} = \frac{\dot{M}_{NO_{abs}}}{\dot{M}_{NO_{em}}}$	NO absorption per coated area $\dot{m}_{NO_{abs}} = \frac{\dot{M}_{NO_{abs}}}{S_p}$ (μg s^{-1} m^{-2})	Normalized NO reduction $NO^* = \frac{NO_{with-ph}}{NO_{without-ph}}$
2	1.7	0.109	0.49	1.24	0.84
3	1.7	0.109	0.41	1.03	0.79
4	0.9	0.057	0.14	0.91	0.84

reduction per painted surface can provide a measure of the capability of a given coating to reduce NO in an urban environment. Then, a normalized NO reduction NO^* has been introduced, where the average over the volume of the street canyon of NO concentration where there is a photocatalytic effect has been divided by the average of NO concentration obtained within the same street canyon with no photocatalytic effect. In the three cases the value of NO* is between 0.79 and 0.84, *i.e.* the photocatalytic effect in the real application shown in this paper gives an average NO reduction within the canyon in the range 14%–20%. On the basis of the results shown in this paper, we can conclude that the photocatalytic coatings can be considered as a passive measure that can help in the challenge of urban pollution mitigation, especially in confined environments such as street canyons where flow recirculation is one of the main effects. Also, the research discussed in this paper can be considered as a framework to test the efficacy of the coatings before their implementation in real scenarios.

Declaration of competing interest

The authors declare that they have no known competing financial interests or personal relationships that could have appeared to influence the work reported in this paper.

Acknowledgements

This work has received funding from the iSCAPE project funded by the European Commission H2020 Research and Innovation programme (H2020-SC5-04-2015) funded under the Grant agreement No. 689954. The authors acknowledge the funding received from the iSCAPE project. This paper reflects the authors' view. The European Commission is not liable for any use that may be made of the information contained therein. The authors would also like to thank Luca Torreggiani, Carla Barbieri and Vanes Poluzzi from ARPAE Environmental Protection Agency, Marco Deserti from Regione Emilia-Romagna, Massimo Bacchetti, Francesca Di Nicola and Martina Polito from the Department of Physics and Astronomy of the University of Bologna, Roberto Carli and the staff of the Department of Civil, Chemical, Environmental and Materials Engineering (DICAM), University of Bologna, for their support in the realization of the experimental field campaign.

Appendix A. Supplementary data

Supplementary data to this article can be found online at https://doi.org/10.1016/j.buildenv.2020.107348.

References

[1] Mills, "Fine Ceramics – Test Method of Air-Purification Performance of Semiconducting Photocatalytic Materials, A. Removal of nitric oxide: Modified ISO 22197-1:2007, Queen's University Belfast, 2007.
[2] A. Folli, I. Pochard, A. Nonat, U.H. Jakobsen, A.M. Shepherd, D.E. Macphee, Engineering photocatalytic cements: understanding TiO2 surface chemistry to control and modulate photocatalytic performances, J. Am. Ceram. Soc. 93 (10) (2010) 3360–3369.
[21] E. Boonen, A. Beeldens, Recent photocatalytic applications for air purification in Belgium, Coatings 4 (3) (2014) 553–573.
[25] M. Janus, K. Zajac, Concretes with photocatalytic activity, in: Yilmaz Salih, Ozmen Hayri Baytan (Eds.), *High Performance Concrete Technology and Applications*,, Open Access Peer-Reviewed Edited, Volume, inTechOpen, 2016, ISBN 978-953-51-2651-5.
[27] J. Lasek, Y.H. Yu, J.C. Wu, Removal of NOx by photocatalytic processes, J. Photochem. Photobiol. C Photochem. Rev. 14 (2013) 29–52.
[3] G.L. Guerrini, Photocatalytic performances in a city tunnel in Rome: NOx monitoring results, Construct. Build. Mater. 27 (2012) 165–175.
[4] M. Gallus, V. Akylas, F. Barmpas, A. Beeldens, E. Boonen, A. Boréave, M. Cazaunau, H. Chen, V. Daële, J.F. Doussin, J.F. Dupart, C. Gaimoz, C. George, B. Grosselin, H. Hermann, S. Ifang, R. Kurtenbach, M. Maille, A. Mellouki, K. Miet, F. Mothes, N. Moussiopoulos, L. Poulain, R. Rabe, P. Zapf, J. Kleffmann, Photocatalytic depollution in the Leopold II tunnel in Brussels: NOx abatement results, Build. Environ. 84 (2015) 125–133.
[5] M.M. Ballari, H.J.H. Brouwers, Full scale demonstration of air-purifying pavement, J. Hazard Mater. 254–255 (2013) 406–414.
[6] Th Maggos, A. Plassais, J.G. Bartzis, Ch Vasilakos, N. Moussiopoulos, L. Bonafous, Photocatalytic degradation of NOx in a pilot street canyon configuration using TiO2-mortar panels, Environ. Monit. Assess. 136 (2008) 35–44.

[8] A.P.R. Jeanjean, J. Gallagher, P.S. Monks, R.J. Leigh, Ranking current prospective NO2 pollution mitigation strategies: an environmental and economic modelling investigation in Oxford Street, London, Environ. Pollut. 225 (2017) 587–597.
[9] A. Jeanjean, R. Buccolieri, J. Eddy, P. Monks, R. Leigh, Air quality affected by trees in real street canyons: the case of Marylebone neighbourhood in central London, Urban For. Urban Green. 22 (2017) 41–53.
[7] S. Di Sabatino, R. Buccolieri, B. Pulvirenti, R. Britter, Simulations of pollutant dispersion within idealised urban-type geometries with CFD and integral models, Atmos. Environ. 41 (2007) 8316–8329.
[11] J.L. Santiago, A. Martilli, F. Martin, On dry deposition modelling of atmospheric pollutants on vegetation at the microscale: application to the impact of street vegetation on air quality, Boundary-Layer Meteorol. 162 (2017) 451–474.
[19] K. Athamena, J.F. Sini, J.M. Rosant, J. Guilhot, Numerical coupling model to compute the microclimate parameters inside a street canyon. Part I: methodology and experimental validation of surface temperature, Sol. Energy 174 (2018) 1237–1251.
[12] M. Palacios, L. Nùñez, M. Pujadas, J. Fernández-Pampillón, M. Germán, B. S. Sánchez, B.S. Cabrero, Estimation of NOx deposition velocities for selected commercial photocatalytic products, WIT Trans. Built Environ. 168 (2015) 729–740.
[24] P.J.M. Hassan, L.N. Mohammad, H. Dylla, S.B. Cooper, A. Mokhtar, S. Asadi, A breakthrough concept in preparation of highly-sustainable photocatalytic warm asphalt mixtures. https://pureti.com/content/documents/PURETI-on-Asphalt—NSF11-Paper-f-Nov-2010-LSU.pdf.
[22] A. Dallman, S. Magnusson, R. Britter, L. Norford, D. Entekhabi, H.J. Fernando, Conditions for thermal circulation in urban street canyons, Build. Environ. 80 (2014) 184–191.
[23] C. Gromke, R. Buccolieri, S. Di Sabatino, B. Ruck, Dispersion study in a street canyon with tree planting by means of wind tunnel and numerical investigations–evaluation of CFD data with experimental data, Atmos. Environ. 42 (37) (2008) 8640–8650.
[28] Klingberg, J., Konarska, J., Lindberg, F., Thorsson, S. 2015. Measured and modelled leaf area of urban woodlands, parks and trees in Gothenburg, Sweden. Presented at the 9th International Conference on Urban Climate (ICUC 9), 20-24 July 2015, available online at: http://www.meteo.fr/icuc9/LongAbstracts/ucp11-6-1881174_a.pdf.
[29] R. Buccolieri, J.-L. Santiago, E. Rivas, B. Sanchez, Review on urban tree modelling in CFD simulations: Aerodynamic, deposition and thermal effects, Urban Forestry & Urban Greening 31 (2018) 212–220, https://doi.org/10.1016/j.ufug.2018.03.003B.
[30] J.H. Amorim, V. Rodrigues, R. Tavares, J. Valente, C. Borrego, CFD modelling of the aerodynamic effect of trees on urban air pollution dispersion, Science of the Total Environment 461–462 (2013) 541–551, https://doi.org/10.1016/j.scitotenv.2013.05.031B.
[13] C. Gromke, B. Blocken, W. Janssen, B. Merema, T. van Hooff, H. Timmermans, CFD analysis of transpirational cooling by vegetation: case study for specific meteorological conditions during a heat wave in Arnhem, Netherlands. Build. Environ 83 (2015) 11–26.
[14] M. Moradpour, H. Afshin, B. Farhanieh, A numerical investigation of reactive air pollutant dispersion in urban street canyon with tree planting, Atmos. Pollut. Res. 8 (2017) 253–266.
[10] S. Di Sabatino, R. Buccolieri, B. Pulvirenti, R. Britter, Simulations of pollutant dispersion within idealised urban-type geometries with CFD and integral models, Atmos. Environ. 41 (2007) 8316–8329.
[20] J.F. Barlow, I.N. Harman, S.E. Belcher, Scalar fluxes from urban street canyons. Part I: laboratory simulation, Boundary-Layer Meteorol. 113 (2004) 369–385.
[31] T. Bentham, R. Britter, Spatially averaged flow within obstacle arrays, Atmospheric Environment 37 (15) (2003) 2037–2043, https://doi.org/10.1016/S1352-2310(03)00123-7.
[15] I.N. Harman, J.F. Barlow, S.E. Belcher, Scalar fluxes from urban street canyons part II: model, Boundary-Layer Meteorol. 113 (3) (2004) 387–410.
[16] R.E. Britter, S.R. Hanna, Flow and dispersion in urban areas, Annu. Rev. Fluid Mech. 35 (1) (2003) 469–496.
[17] P. Kastner-Klein, R. Berkowicz, R. Britter, The influence of street architecture on flow and dispersion in street canyons, Meteorol. Atmos. Phys. 87 (1–3) (2004) 121–131.
[26] A. Kubilay, M.K.A. Neophytou, S. Matsentides, M. Loizou, J. Carmeliet, The pollutant removal capacity of an urban street canyon and its link to the breathability and exchange velocity, Procedia Eng. 180 (2017) 443–451, https://doi.org/10.1016/j.proeng.2017.04.203.
[18] J. Stocker, C. Hood, D. Carruthers, C. McHugh, ADMS-Urban: developments in modelling dispersion from the city scale to the local scale, Int. J. Environ. Pollut. 50 (2012) 308–316.